

# Properties of active rectifier with LCL filter in the selection process of the weighting factors in finite control set-MPC

P. FALKOWSKI\*, A. SIKORSKI, K. KULIKOWSKI, and M. KORZENIEWSKI

Department of Power Electronics and Electric Drives, Białystok University of Technology, 45D Wiejska St., 15-351 Białystok, Poland

**Abstract.** One of the main problems of multivariable cost functions in model predictive control is the choice of weighting factors. Two finite control set model predictive control algorithms, applied to the three-phase active rectifier with an LCL filter, are described in the paper. The investigated algorithms, i.e.  $PC_{i_c u_c}$  and  $PC_{i_g i_c u_c}$ , implement multivariable approaches applying line (grid) current, capacitor voltage and converter current. The main problem dealt with in the paper is the choice of optimum values of the cost function weighting factors. The values of the factors calculated using the method proposed in the paper are very close to the values represented by the lowest THDi of the line current. Moreover, simulations verifying the equations used in the prediction of controlled values, i.e. line current, capacitor voltage and converter current, are presented. Both simulation and experimental results are presented to verify effectiveness of the investigated control strategies under change of the load ( $P = 5$  kW and 2.5 kW), during transient states, under unbalanced and balanced line voltage.

**Key words:** model predictive control (MPC), active front end (AFE) converters, inductive-capacitive-inductive (LCL) filter, weighting factors selection.

## 1. Introduction

As the processing power of digital signal processors (DSP) increased, so did the interest in model predictive control (MPC) [1]. Predictive control methods can be classified into two basic groups: finite control set-MPC (FCS-MPC) and continuous control set-MPC (CCS-MPC) [2].

The FCS-MPC algorithm utilizes the digital character of power electronic converters, distinguished by a finite number of voltage vectors for prediction of future behavior of regulated variables. For all voltage vectors, computations are carried out in any sampling period. The optimum switching combination is chosen in order to minimize the determined cost function  $J$ , which allows to simultaneously control several parameters in the converter, such as voltages [3], currents [4], flux and torque [5], average switching frequency of transistors [6], CM voltages [7, 8] and speed [9]. Such properties were utilized to control methods presented in this article. With the wide range of possibilities in setting out the cost function, the FCS-MPC algorithm has been used for varied kinds of inverters such as multilevel inverters [10], current source converters [11] and active filters [12].

Commonly, three-phase active rectifiers are connected to the AC line by one of two types of passive filters: the first-order – L filter, or the third-order – LCL filter (consisting of line-side inductance, capacitance and converter-side inductance). The LCL filter manifests better ripple damping as compared with simple L inductance [13]. Therefore, the overall value of inductors re-

quired is diminished, which also minimizes the cost and size of the inverter. Nevertheless, the LCL filter generates resonance, which should to be suppressed [14].

In [15], the authors propose two FCS-MPC methods: one that uses cost function  $J$  to control two parameters of the LCL filter and the another, which controls the line current directly. These methods allow to suppress the harmonics around LCL resonance and to obtain low line current total harmonic distortion (THDi) with low mean switching frequency  $f_{sw(av)}$ .

The methods described in [16] use more than two variables in the cost function. In  $PC_{i_g i_c u_c}$  control, an entire model of the LCL filter is used to predict change in the three controlled parameters – converter current vector  $i_c$ , line (grid) current vector  $i_g$  and capacitor voltage vector  $u_c$  of the LCL filter. Compared to the existing methods, the authors have proposed an alternative way to compute the reference capacitor voltage and the converter current based on the reference grid current. This allows all states to be considered in the cost function instead of using only the system output to act as the controller, i.e. grid current. Investigations have shown that the algorithm guarantees very effective performance in both transient and steady states.

The presence of weighting factors in the cost function  $J$  is due to the fact that simultaneous control of many different variables (i.e. ones that have different units, values or rate of variation) in one cost function  $J$  requires coefficients to scale the above-mentioned differences [17]. In other words, weighting factors are there to unify the influence of the very different physical quantities on the choice of the converter voltage vector. What is more, weighting factors allow to change the preferences concerning the quality of regulation of values in the cost function, i.e. their values directly influence the quality of control. The criteria for the choice of weighting factors are

\*e-mail: p.falkowski@pb.edu.pl

Manuscript submitted 2019-08-09, revised 2019-10-04, initially accepted for publication 2019-10-28, published in February 2020

more ambiguous than the choice of optimum values for PI controllers. These controllers have been known and used in power electronics and electric drive for decades. Numerous different criteria for the choice of linear controller setting have been developed [18].

The choice of the values of weighting factors has been widely discussed and developed in recent years [1, 2]. Publications [17] and [19] present prediction methods in which the values of weighting factors in the cost function were chosen empirically based on simulations. Genetic algorithms [20] as well as fuzzy logic [21] and the criteria for minimization of mean squared error (MSE) [22] proved to be useful in the choice of the values of weighting factors. Publications [23] and [24] describe algorithms which lack weighting factors in the function  $J$ . The automated tuning of weighting factors using an artificial neural network for uninterruptible power supply was proposed in [25].

The algebraic tuning guidelines for model predictive torque and flux control have been discussed in [26]. The author has considered an asynchronous machine supplied by a three-level neutral point clamped inverter. The algebraic design guidelines were stated in [26] to achieve minimum torque, flux and current ripple per switching frequency.

In the further part of this paper, a method which allows to estimate the values of weighting factors in algorithms  $PCi_c u_c$  and  $PCi_g i_c u_c$  is presented. The proposed solution does not produce unambiguous values that will allow to obtain the best control effect. However, this method narrows down the set of optimum values of weighting factors to a considerable extent. Moreover, simulations verifying the equations used in the prediction of controlled values, i.e. line current, capacitor voltage and converter current, are presented. The paper demonstrates simulation and experimental results which prove that the values of the weighting factors selected using the proposed method allow to work with varying power ( $P = 5$  kW and  $P = 2.5$  kW), during transient states, under unbalanced and balanced line voltage ( $E_a = 0.75E_n$ ).

The organization of the paper is as follows. In Section 2, a scheme of the converter is presented. Section 3 presents equations used for the calculation of the cost function of methods  $PCi_c u_c$  and  $PCi_g i_c u_c$  as well as their evaluation in simulations. Section 4 presents an original method of selection of weighting factors in the cost function. The method has been verified by means of simulations. In Section 5, the proper selection of weighting factors is further confirmed by laboratory tests. Finally, the general conclusions are summarized in Section 6.

## 2. Modeling of 2-level AC/DC-LCL converter

Figure 1 shows the three-phase active rectifier (converter) linked to the line (grid) using a passive LCL filter. The active rectifier can be described by relationships (1)–(3) within the  $dq$  rotating reference frame:

$$L_g \frac{d}{dt} \mathbf{i}_{gdq} = \mathbf{e}_{dq} - j\omega_g L_g \mathbf{i}_{gdq} - \mathbf{u}_{cdq}, \quad (1)$$

$$L_c \frac{d}{dt} \mathbf{i}_{cdq} = \mathbf{u}_{cdq} - j\omega_g L_c \mathbf{i}_{cdq} - \mathbf{u}_{dq}, \quad (2)$$

$$C \frac{d}{dt} \mathbf{u}_{cdq} = \mathbf{i}_{gdq} - \mathbf{i}_{cdq} - j\omega_g C \mathbf{u}_{cdq}, \quad (3)$$

where:

$\mathbf{i}_{gdq}$  – grid current vector in the rotating  $dq$  reference frame,

$\mathbf{i}_{cdq}$  – converter current vector in the rotating  $dq$  reference frame,

$\mathbf{e}_{dq}$  – line (grid) voltage vector in the rotating  $dq$  reference frame,

$\mathbf{u}_{cdq}$  – filter capacitance  $C$  voltage vector in the rotating  $dq$  reference frame,

$L_g$  – line (grid) side inductor,

$L_c$  – converter side inductor,

$C$  – filter capacitor,

$\omega_g$  – line (grid) angular frequency,

$$\mathbf{u}_{dq} = \begin{cases} \frac{2}{3} U_{DC} e^{j[(i-1)\frac{\pi}{3} - \omega_g t]} & \text{for } i = \{1, 2, 3, 4, 5, 6\} \\ "0" & \text{for } i = \{0, 7\} \end{cases}$$

– converter output vector in the rotating  $dq$  reference frame.

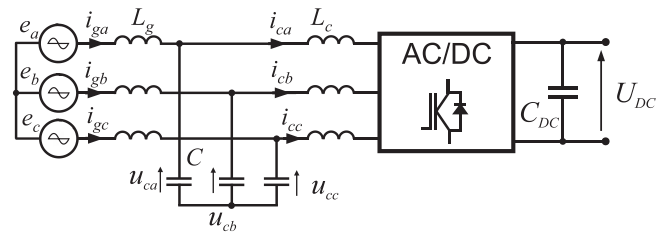


Fig. 1. Schematic diagram of active rectifier with LCL filter

Figure 2 presents an equivalent circuit diagram described by relationships (1)–(3). Table 1 contains the parameters of the simulation and experimental model.

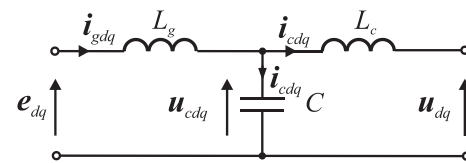


Fig. 2. Circuit diagram of LCL filter in  $dq$  rotating reference frame

Table 1  
System parameters

Variable	Parameters	Value
$E$	Grid voltage	325 V
$U_{DC}$	DC capacitor voltage	650 V
$T_s (f_s)$	Sampling time (sampling frequency)	25 $\mu$ s (40 kHz)
$L_g$	Grid-side inductor	1.8 mH
$L_c$	Converter-side inductor	3.4 mH
$C$	Filter capacitor	20 $\mu$ F
$f_r$	$L_g$ – $C$ – $L_c$ filter resonance frequency	1037 Hz

### 3. Control algorithms

**3.1. PC<sub>i<sub>c</sub>u<sub>c</sub></sub>** algorithm. The active damping algorithm [27, 28] is the most universal method of damping line current distortions (oscillations connected with resonance frequency  $f_{rg}$ ). It is based on the virtual damping resistance  $R_d$  parallel to the capacitor  $C$  of the LCL filter, which decreases additional power losses. The general drawback of the active damping algorithm is its low immunity to line voltage disruptions. The appearance of higher harmonics or asymmetry of line voltage results in deformation of the line currents [15, 16, 27].

An alternative approach to damping harmonics around LCL resonance is to implement simultaneous control of two filter parameters, i.e. converter current  $i_c$  and capacitance voltage  $u_c$ . An algorithm named PC<sub>i<sub>c</sub>u<sub>c</sub></sub> was presented in [29] and similarly in [15]. Apart from superior resistance to disruptions appearing in the line voltage, it also permits to achieve better quality of the line current in the steady state at the same mean switching frequency of transistors in comparison to the active damping method [15, 29].

The PC<sub>i<sub>c</sub>u<sub>c</sub></sub> method works based on the scheme depicted in Fig. 3. Applying the set line current vector  $\mathbf{i}_{gdq}^*$ , it is possible to determine the set values of the capacitance voltage vector (4) and next the inverter current vector (5).

$$\mathbf{u}_{cdq}^* = \mathbf{e}_{dq} - j\omega_g L_g \mathbf{i}_{gdq}^*, \quad (4)$$

$$\mathbf{i}_{cdq}^* = \mathbf{i}_{gdq}^* - j\omega_g C \mathbf{u}_{cdq}^*. \quad (5)$$

For sufficiently short sampling time  $T_s$ , it can be assumed that:

$$\mathbf{u}_{cdq}^*(n+1) \approx \mathbf{u}_{cdq}^*(n), \quad (6)$$

$$\mathbf{i}_{cdq}^*(n+1) \approx \mathbf{i}_{cdq}^*(n). \quad (7)$$

This assumption has been applied to all the control algorithms discussed in this article.

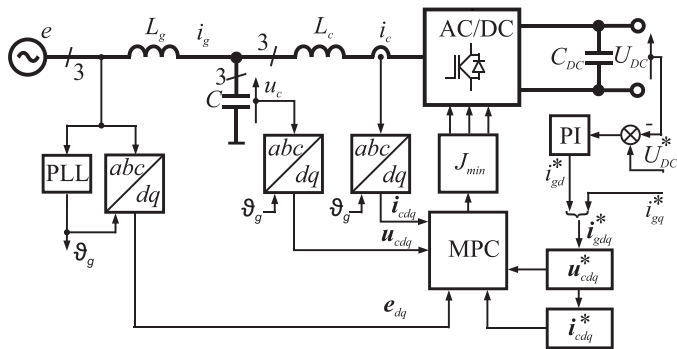


Fig. 3. Schematic diagram of PC<sub>i<sub>c</sub>u<sub>c</sub></sub> control method

Prediction algorithm starts and measures the real values of currents and voltages (step  $n$ ). Considering  $T_s$  as the sampling time, the converter current derivative is obtained by means of the Euler forward method:

$$\frac{d}{dt} \mathbf{i}_{cdq} \approx \frac{\Delta \mathbf{i}_{cdq}(n+1)}{T_s} = \frac{\mathbf{i}_{cdq}(n+1) - \mathbf{i}_{cdq}(n)}{T_s}. \quad (8)$$

Taking account of formula (2), the predicted converter current vector  $\mathbf{i}_{cdq}(n+1)$  can be expressed as:

$$\Delta \mathbf{i}_{cdq}(n+1) = \frac{\mathbf{u}_{cdq}(n) - j\omega_g L_c \mathbf{i}_{cdq}(n) - \mathbf{u}_{dq}(n+1)}{L_c} T_s, \quad (9)$$

$$\mathbf{i}_{cdq}(n+1) = \mathbf{i}_{cdq}(n) + \Delta \mathbf{i}_{cdq}(n+1) \quad (10)$$

Assuming that:

$$\frac{d}{dt} \mathbf{u}_{cdq} \approx \frac{\Delta \mathbf{u}_{cdq}(n+1)}{T_s} = \frac{\mathbf{u}_{cdq}(n+1) - \mathbf{u}_{cdq}(n)}{T_s}, \quad (11)$$

the next capacitance voltage vector  $\mathbf{u}_{cdq}(n+1)$  can be obtained:

$$\begin{aligned} \Delta \mathbf{u}_{cdq}(n+1) &= \\ &= \frac{\mathbf{i}_{gdq}(n) - j\omega_g C \mathbf{u}_{cdq}(n) - \mathbf{i}_{cdq}(n) - 0.5 \Delta \mathbf{i}_{cdq}(n+1)}{C} T_s, \end{aligned} \quad (12)$$

$$\mathbf{u}_{cdq}(n+1) = \mathbf{u}_{cdq}(n) + \Delta \mathbf{u}_{cdq}(n+1). \quad (13)$$

Changes in voltage  $\mathbf{u}_{cdq}$  are essentially dependent on the current  $\mathbf{i}_{cdq}$  that alters from  $\mathbf{i}_{cdq}(n)$  to  $\mathbf{i}_{cdq}(n+1)$ . Nevertheless, its mean value, in the sampling time  $T_s$  equals  $(\mathbf{i}_{cdq}(n) + 0.5 \Delta \mathbf{i}_{cdq}(n+1))$ . The factor 0.5 in equation (12) is in charge of “averaging” the change of the current vector  $\Delta \mathbf{i}_{cdq}$  in period  $T_s$ . The change results in the alteration of the capacitor voltage vector  $\Delta \mathbf{u}_{cdq}(n+1)$ .

Afterwards, expected errors of controlled variables are determined:

$$\boldsymbol{\varepsilon}_{icdq}(n+1) = \mathbf{i}_{cdq}^*(n+1) - \mathbf{i}_{cdq}(n+1), \quad (14)$$

$$\boldsymbol{\varepsilon}_{ucdq}(n+1) = \mathbf{u}_{cdq}^*(n+1) - \mathbf{u}_{cdq}(n+1). \quad (15)$$

In the last part of the prediction, applying the cost function  $J$ , the determination of the optimum voltage vector of converter  $\mathbf{u}_{dq}(n+1)$  is performed:

$$\begin{aligned} J &= w_{uc}^2 (\boldsymbol{\varepsilon}_{ucd}^2(n+1) + \boldsymbol{\varepsilon}_{ucq}^2(n+1)) + \\ &+ (\boldsymbol{\varepsilon}_{icd}^2(n+1) + \boldsymbol{\varepsilon}_{icq}^2(n+1)). \end{aligned} \quad (16)$$

A 2-level converter delivers eight voltage vectors: six active vectors and two zero vectors (“111” and “000”). Computations of cost function  $J$  are made for seven vectors. If the “0” voltage vector is selected as the optimum one, in order to minimize the transistors’ switching frequency  $f_{sw}$ , the selection between “000” or “111” is made.

It is often the case that authors in publications omit the verification of equations used for the prediction of controlled quantities. Therefore, Fig. 4 and Fig. 5 present the results of the algorithm for calculating the predicted converter current vector  $\mathbf{i}_{cdq}(n+1)$  (Fig. 4) and capacitor voltage vector  $\mathbf{u}_{cdq}(n+1)$  (Fig. 5). As the waveforms show, the values  $\mathbf{i}_{cdq}(n+1)$  and  $\mathbf{u}_{cdq}(n+1)$ , determined in step  $n$ , closely overlap with the values of current  $\mathbf{i}_{cdq}$  and voltage  $\mathbf{u}_{cdq}$  in step  $(n+1)$ . The “measured” values of the vector  $\mathbf{i}_{cdq}$  and  $\mathbf{u}_{cdq}$  components have been rendered in Matlab/Simulink with the step of 0.1  $\mu$ s.

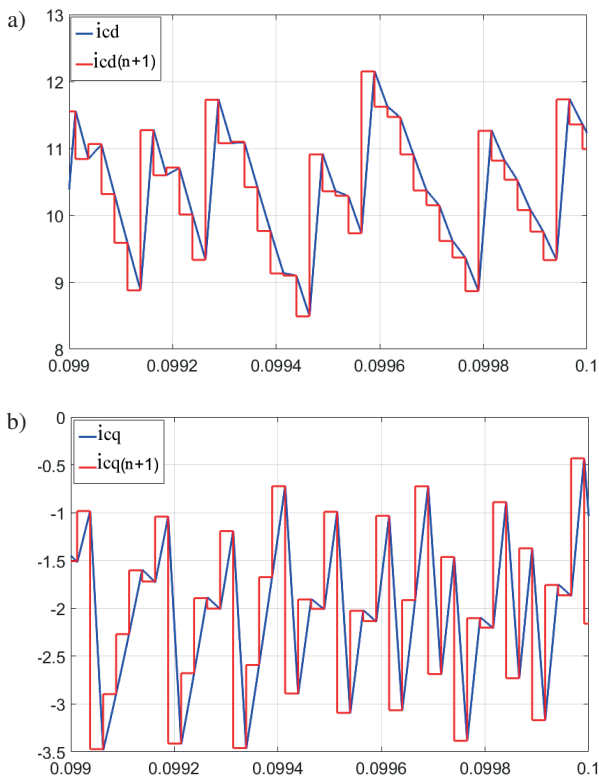


Fig. 4. Waveform of the predicted current  $i_{cdq}(n+1)$  (0.5 A/div) vector and the “measured” current  $i_{cdq}$  (0.5 A/div) value: a) component  $d$ ; b) component  $q$

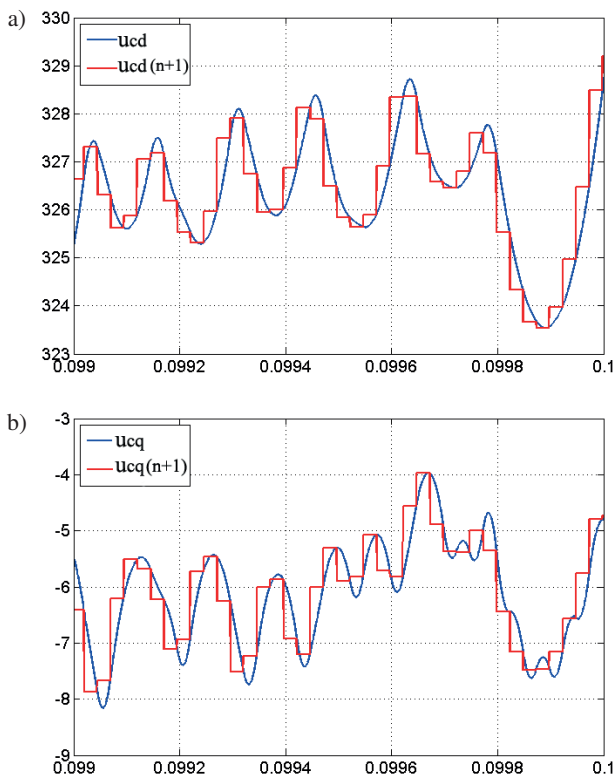


Fig. 5. Waveform of the predicted voltage vector  $u_{cdq}(n+1)$  (1 V/div) and the “measured” voltage value  $u_{cdq}$  (1 V/div) value: a) component  $d$ ; b) component  $q$

Figure 6 presents an oscillogram of phase voltage  $e_a$  and phase current  $i_{ga}$  in a steady state.  $THD_i$  of the phase current equals 1.9%. The  $PCi_c u_c$  algorithm allowed to obtain a substantial minimized value of resonance harmonics of the LCL filter in the line current.

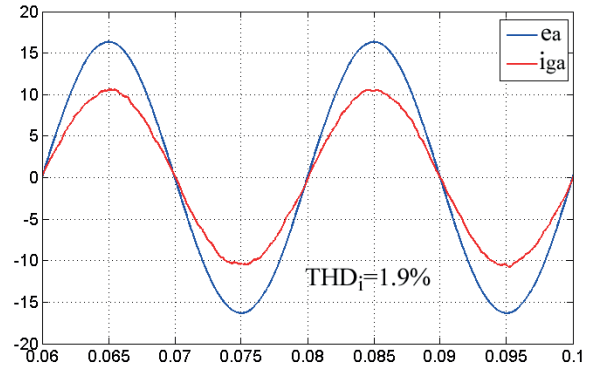


Fig. 6. Line phase voltage  $e_a$  (100 V/div) and current  $i_{ga}$  (5 A/div) for  $PCi_c u_c$  algorithm (simulations results)

**3.2.  $PCi_g i_c u_c$  algorithm.** The control method described in the previous subchapter ( $PCi_c u_c$ ) uses the main advantage of FCS-MPC algorithms, i.e. the fact that various control parameters can be parallelly controlled by a single cost function. The results that have been obtained encouraged the authors to conduct further research aimed at finding new ways to improve the properties of the  $PCi_c u_c$  method. Taking one step ahead, one could expand the cost function  $J$  (16) to include additional direct control of the line current  $i_g$ . Algorithm  $PCi_g i_c u_c$  [16], i.e. predictive control of the line current  $i_g$ , the current of the converter  $i_c$ , and the voltage on the capacitor  $u_c$  could all be monitored in this manner. A block diagram of the  $PCi_g i_c u_c$  control algorithm is shown in Fig. 7.

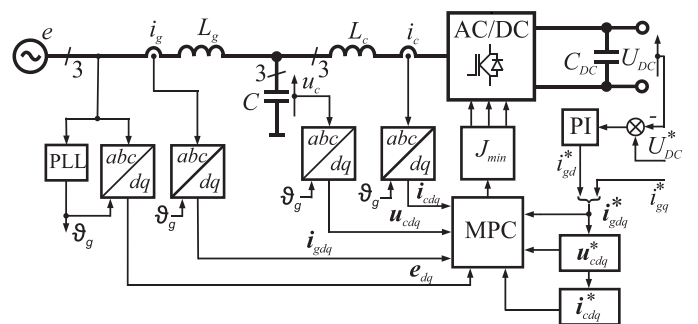


Fig. 7. Schematic diagram of  $PCi_g i_c u_c$  control algorithm

Using the set line current vector  $i_{gdq}^*$ , the set values of the capacitance voltage vector can be expressed as (4) and those of the converter current vector by (5). Applying previous assumptions (6)–(7) and assuming sufficiently short time  $T_s$ , it can be considered that:

$$i_{gdq}^*(n+1) \approx i_{gdq}^*(n). \quad (17)$$

The future current converter vector  $i_{cdq}(n+1)$  and capacitance voltage vector  $u_{cdq}$  are determined using equations (8)–(13).

The predicted line current vector  $\mathbf{i}_{gdq}(n+1)$  is calculated by the following equation:

$$\Delta \mathbf{i}_{gdq}(n+1) = \frac{\mathbf{e}_{dq}(n) - j\omega_g L_g \mathbf{i}_{gdq}(n) - \mathbf{u}_{cdq}(n) - 0.5\Delta \mathbf{u}_{cdq}(n+1)}{L_g} T_s, \quad (18)$$

$$\mathbf{i}_{gdq}(n+1) = \mathbf{i}_{gdq}(n) + \Delta \mathbf{i}_{gdq}(n+1). \quad (19)$$

Changes in current  $\mathbf{i}_{gdq}$  depend on voltage  $\mathbf{u}_{cdq}$ , which that oscillates between the range of  $\mathbf{u}_{cdq}(n)$  to  $\mathbf{u}_{cdq}(n+1)$ . Nevertheless, its mean value, over time  $T_s$ , equals  $(\mathbf{u}_{cdq}(n) + 0.5\Delta \mathbf{u}_{cdq}(n+1))$ . The factor 0.5 in equation (18) is in charge of “averaging” the change of the voltage vector  $\Delta \mathbf{u}_{cdq}$  over the period  $T_s$ . The change causes the alteration of the line current vector  $\Delta \mathbf{i}_{gdq}(n+1)$ .

Afterwards, expected errors of controlled variables are determined:

$$\boldsymbol{\varepsilon}_{icdq}(n+1) = \mathbf{i}_{cdq}^*(n+1) - \mathbf{i}_{cdq}(n+1), \quad (20)$$

$$\boldsymbol{\varepsilon}_{ucdq}(n+1) = \mathbf{u}_{cdq}^*(n+1) - \mathbf{u}_{cdq}(n+1), \quad (21)$$

$$\boldsymbol{\varepsilon}_{igdq}(n+1) = \mathbf{i}_{gdq}^*(n+1) - \mathbf{i}_{gdq}(n+1). \quad (22)$$

The last step implementation of the method is introduced to provide optimum control of the converter voltage vector  $\mathbf{u}_{dq}(n+1)$ . The determinations of  $J$  (23) are performed for all voltage vectors, with reference to the switching optimization applied for the PCi<sub>c</sub>u<sub>c</sub> algorithm.

$$J = w_{ig}^2 (\boldsymbol{\varepsilon}_{igd}^2(n+1) + \boldsymbol{\varepsilon}_{igq}^2(n+1)) + w_{uc}^2 (\boldsymbol{\varepsilon}_{ucd}^2(n+1) + \boldsymbol{\varepsilon}_{ucq}^2(n+1)) + (\boldsymbol{\varepsilon}_{icd}^2(n+1) + \boldsymbol{\varepsilon}_{icq}^2(n+1)). \quad (23)$$

Basing on simulation tests, Fig. 8 shows the verification of the algorithm for calculating the expected line current vector  $\mathbf{i}_{gdq}(n+1)$ . The waveforms show that the predicted values  $\mathbf{i}_{gdq}(n+1)$  determined in step  $n$  closely overlap with the values of current  $\mathbf{i}_{gdq}$ . The “measured” values of the vector  $\mathbf{i}_{gdq}$  components have been rendered in Matlab/Simulink with the step of 0.1  $\mu$ s. Figure 9 presents line current and voltage waveforms for weighting factors  $w_{uc} = 1.0$  and  $w_{ig} = 24.3$ . The THD<sub>i</sub> value of  $i_{ga}$  is 1.3%.

## 4. Selection of the weighting factor values

**4.1. Method of pre-selecting weighting factor values.** One of the main disadvantages of FCS-MPC control is the necessity of selecting weighting factors in the cost function. However, in comparison to the selection of settings for PI controllers, this task is more complicated. To the authors’ knowledge, no universal method of calculating optimum weighting factors has been presented to date. Therefore, an approach to the approximate determination of the factor values, useful in the above algorithms, is presented below.

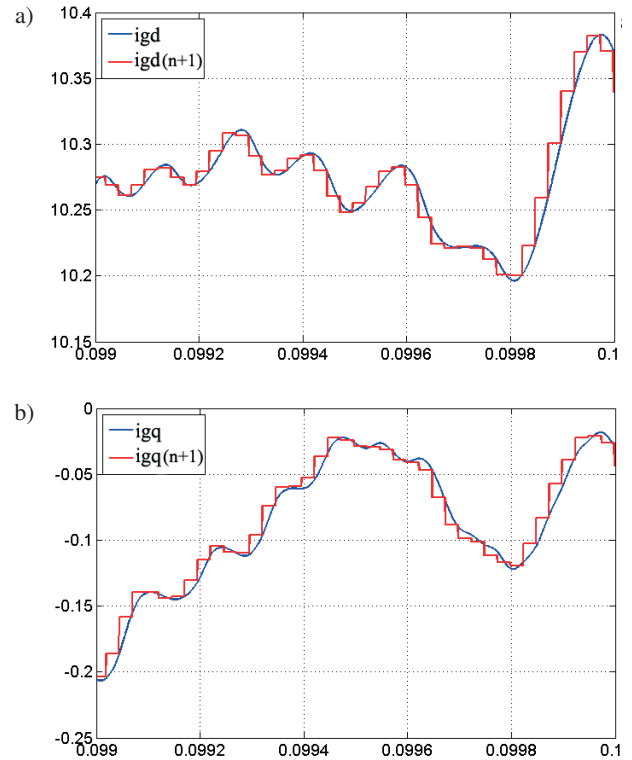


Fig. 8. Waveform of the predicted current  $\mathbf{i}_{gdq}(n+1)$  (50 mA/div) vector and the “measured” current  $\mathbf{i}_{ggdq}$  (50 mA/div) value: a) component d; b) component q

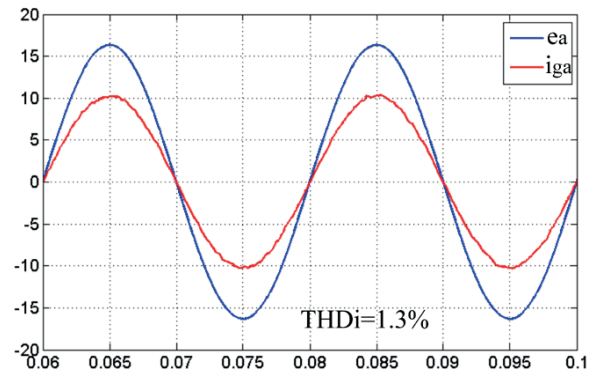


Fig. 9. Line phase current  $i_{ga}$  (5 A/div) and voltage  $e_a$  (100 V/div) for PCi<sub>g</sub>i<sub>c</sub>u<sub>c</sub> algorithm (simulations results)

The proposed cost functions  $J$  (16) and  $J$  (23) consist of the errors of two (PCi<sub>c</sub>u<sub>c</sub>) or three (PCi<sub>g</sub>i<sub>c</sub>u<sub>c</sub>) controlled variables ( $\mathbf{i}_{gdq}$ ,  $\mathbf{i}_{cdq}$ ,  $\mathbf{u}_{cdq}$ ). Factor  $w_{uc}$  affects the suppressing level of resonance frequency, while factor  $w_{ig}$  determines the quality of the set line current reconstruction. Those variables have a different character (different units and magnitudes, different rates of change). Quantity  $\Delta \mathbf{i}_{cdq}(n+1)$  in one sampling period  $T_s$  undergoes a relatively largest change whereas for  $\Delta \mathbf{i}_{gdq}(n+1)$  the change is relatively smallest. The size of the changes translates into the size of error vectors  $\boldsymbol{\varepsilon}$  in the cost functions  $J$  (16) and  $J$  (23). In view of the above, it is essential to use weighting factors to regulate the impact of variables on the value of the cost

function. Equations (20)–(22) define how the predicted values of errors were calculated. They could also be presented in the following form:

$$\begin{aligned} \boldsymbol{\varepsilon}_{icdq}(n+1) &= \mathbf{i}_{cdq}^*(n+1) - \mathbf{i}_{cdq}(n+1) = \\ &= \mathbf{i}_{cdq}^*(n+1) - (\mathbf{i}_{cdq}(n) + \Delta\mathbf{i}_{cdq}(n+1)), \end{aligned} \quad (24)$$

$$\begin{aligned} \boldsymbol{\varepsilon}_{ucdq}(n+1) &= \mathbf{u}_{cdq}^*(n+1) - \mathbf{u}_{cdq}(n+1) = \\ &= \mathbf{u}_{cdq}^*(n+1) - (\mathbf{u}_{cdq}(n) + \Delta\mathbf{u}_{cdq}(n+1)), \end{aligned} \quad (25)$$

$$\begin{aligned} \boldsymbol{\varepsilon}_{igdq}(n+1) &= \mathbf{i}_{gdq}^*(n+1) - \mathbf{i}_{gdq}(n+1) = \\ &= \mathbf{i}_{gdq}^*(n+1) - (\mathbf{i}_{gdq}(n) + \Delta\mathbf{i}_{gdq}(n+1)). \end{aligned} \quad (26)$$

Assuming that the control method ensures that the controlled values  $\mathbf{i}_{gdq}$ ,  $\mathbf{i}_{cdq}$ ,  $\mathbf{u}_{cdq}$  are close to the set values  $\mathbf{i}_{gdq}^*$ ,  $\mathbf{i}_{cdq}^*$ ,  $\mathbf{u}_{cdq}^*$ , equations (24)–(26) can be simplified to:

$$\boldsymbol{\varepsilon}_{icdq}(n+1) = -\Delta\mathbf{i}_{cdq}(n+1), \quad (27)$$

$$\boldsymbol{\varepsilon}_{ucdq}(n+1) = -\Delta\mathbf{u}_{cdq}(n+1), \quad (28)$$

$$\boldsymbol{\varepsilon}_{igdq}(n+1) = -\Delta\mathbf{i}_{gdq}(n+1). \quad (29)$$

Weighting factors  $w_{ig}$  and  $w_{uc}$  are there to unify/“align” the changes of the grid current  $\Delta\mathbf{i}_{gdq}$  and the capacitor voltage  $\Delta\mathbf{u}_{cdq}$  with the changes of the converter current  $\Delta\mathbf{i}_{cdq}$  in sampling time  $T_s$ . Using the cost function (23) and equations (27)–(29), changes of the converter current  $\Delta\mathbf{i}_{cdq}$  are compared capacitor voltage changes  $\Delta\mathbf{u}_{cdq}$  and, separately, changes of the converter current  $\Delta\mathbf{i}_{cdq}$  are compared with grid current changes  $\Delta\mathbf{i}_{gdq}$ :

$$w_{uc} |\Delta\mathbf{u}_{cdq}(n+1)| = |\Delta\mathbf{i}_{cdq}(n+1)|, \quad (30)$$

$$w_{ig} |\Delta\mathbf{i}_{gdq}(n+1)| = |\Delta\mathbf{i}_{cdq}(n+1)|. \quad (31)$$

Transformations (30)–(31) allow for preliminary estimation of weighting factors by relating the largest changes of the controlled values that are possible to be achieved during one sampling period  $T_s$ :

$$w_{uc} \approx \sqrt{\frac{|\Delta\mathbf{i}_{cdq}(n+1)|}{|\Delta\mathbf{u}_{cdq}(n+1)|}}, \quad (32)$$

$$w_{ig} \approx \sqrt{\frac{|\Delta\mathbf{i}_{cdq}(n+1)|}{|\Delta\mathbf{i}_{gdq}(n+1)|}}. \quad (33)$$

$\Delta\mathbf{i}_{cdq}(n+1)$ ,  $\Delta\mathbf{u}_{cdq}(n+1)$  and  $\Delta\mathbf{i}_{gdq}(n+1)$  are determined using equations (9), (12) and (18) for the converter voltage vector module  $|\mathbf{u}_{dq}| = 2/3 U_{DC}$ . The value of the weighting factor is a root of the quotient of the analyzed changes because a series of simulation tests showed that this improves the accuracy of estimating the values of the factors that provide for best control quality. This way, the choice of the converter voltage vector is mainly influenced by the inverter current error vector, whereas the influence of the error vectors of the capacitor voltage and converter current is smaller. The given relationships

allow for initial estimation of the weighting factors, which in turn speeds up the implementation process of the methods being developed.

**4.2. Verification of the method of pre-selection of weighting factors.** In order to verify the usefulness of the above-described method of selecting weights, a number of simulation tests was carried out to measure the THD<sub>i</sub> value of line current  $i_g$ . The values of factors calculated according to the above-mentioned relations were presented in Table 2. The calculated weight factor values were named as nominal values. Figure 10 shows how the THD<sub>i</sub> value of line current  $i_g$  changed depending on the change of the weighting factor  $w_{uc}$  for the PCi<sub>c</sub>u<sub>c</sub> method. The calculated nominal value (Table 2) was  $w_{ucN1} = 1.25$  with THD<sub>i</sub> = 2.1%. The lowest THD<sub>i</sub> = 1.9% was noted for  $w_{uc} = 0.8w_{ucN1}$ . Lowering the  $w_{uc}$  below  $0.6w_{ucN1}$  causes the increase of THD<sub>i</sub>. The values of  $w_{uc}$  higher than  $w_{ucN1}$  also cause the increase of THD<sub>i</sub> of the line current.

Table 2  
Calculated nominal values of weighting factors

Variable	Parameters	Value
$w_{ucN1}$	Nominal value of weighting factor $w_{uc}$ for LCL filter from Table 1	1.25
$w_{igN1}$	Nominal value of weighting factor $w_{ig}$ for LCL filter from Table 1	15.2

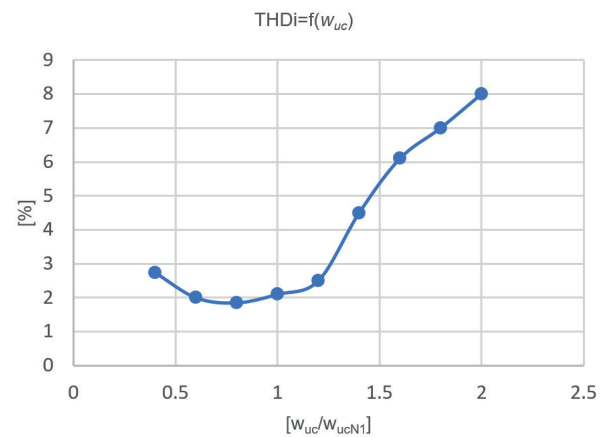


Fig. 10. THD<sub>i</sub> of the grid current  $i_g$  with the changing weight  $w_{uc}$  for the PCi<sub>c</sub>u<sub>c</sub> method. The parameters of the LCL filter and the converter as in Table 1

Apart from the  $w_{uc}$ , the PCi<sub>c</sub>i<sub>c</sub>u<sub>c</sub> method includes one more weighting factor, i.e.  $w_{ig}$ . The nominal value calculated from the data from Table 1 was  $w_{igN1} = 15.2$  (Table 2). Basing on the results from Fig. 10, it was assumed that  $w_{uc} = 0.8w_{ucN1}$ . Lowering the value of  $w_{ig}$  below  $w_{igN1}$  causes the increase of THD<sub>i</sub> of the line current (Fig. 11), whereas increasing it to  $1.6w_{igN1}$  allows to achieve a better shape of the line current. The lowest THD<sub>i</sub> = 1.3% is noted for  $w_{ig} = 1.6w_{igN1}$ .  $w_{ig}$  values above  $1.6w_{igN1}$  cause THD<sub>i</sub> of the line current to rise again.

Properties of active rectifier with LCL filter in the selection process of the weighting factors in finite control set-MPC

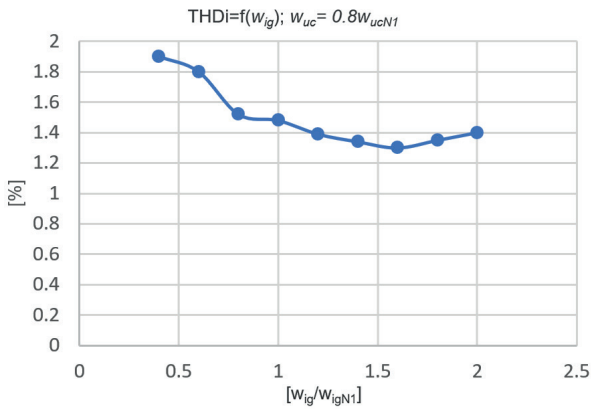


Fig. 11. THD<sub>i</sub> of the grid current  $i_g$  with the changing weight  $w_{ig}$  for the PC<sub>igicuc</sub> method. The value of the other weighting factor was constant  $w_{uc} = 0.8w_{ucN}$ . The parameters of the LCL filter and the converter as in Table 1

Figure 12 shows line phase voltage  $e_a$  and line current waveforms  $i_g$  with step changes of the weighting factor  $w_{uc}$  for the PC<sub>icuc</sub> method. With  $w_{uc} = 0.4w_{ucN1}$  weaker damping of the resonant frequency  $f_{rg}$  of the LCL filter can be observed. With  $w_{uc} = 1.6w_{ucN1}$ , distortion of the line current increases and, moreover, the converter operates with a non-unity power factor.

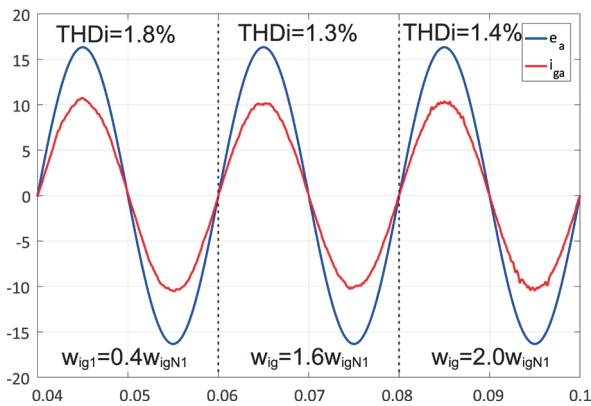


Fig. 12. Line phase voltage  $e_a$  (100 V/div) and current  $i_{ga}$  (5 A/div) for PC<sub>icuc</sub> algorithm while step changes of the  $w_{uc}$  factor

Figure 13 shows voltage  $e_a$  and current  $i_g$  with step changes of the weighting factor  $w_{ig}$  for the PC<sub>igicuc</sub> method. The value of  $w_{uc} = 0.8w_{ucN1}$  was not changed. When  $w_{ig}$  is small and equal to  $0.4w_{igN1}$ , the choice of the voltage vector in the cost function  $J$  (23) is influenced mainly by the error vectors  $\epsilon_{icdq}$  and  $\epsilon_{ucdq}$ . The PC<sub>igicuc</sub> method behaves similarly to PC<sub>icuc</sub>. When  $w_{ig}$  is larger than  $2.0w_{igN1}$ , THD<sub>i</sub> of the line current increases.

Subsequently, simulations which verify the operation of control algorithms were carried out for two active powers (5.0 kW and 2.5 kW). They used the weighting factors calculated in the way presented herein, whose values were  $w_{uc} = 1.0$  (PC<sub>icuc</sub>) as well as  $w_{uc} = 1.0$  and  $w_{ig} = 24.3$  (PC<sub>igicuc</sub>).

Figure 14 shows waveforms of grid voltage  $e_a$  and current  $i_g$ . As we can see, the selected values of the weighting factors provide a low THD<sub>i</sub> of the grid current regardless of the active

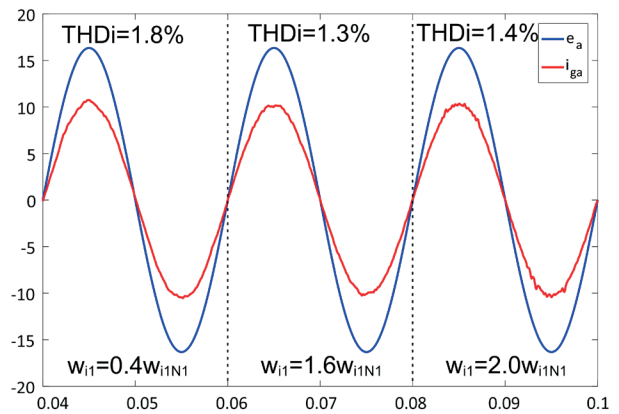


Fig. 13. Line phase voltage  $e_a$  (100 V/div) and current  $i_{ga}$  (5 A/div) for PC<sub>igicuc</sub> algorithm while step changes of the  $w_{ig}$  factor. The value of  $w_{uc}$  was constant and equal to  $0.8w_{ucN}$

power values for both control algorithms, with a lower value obtained for the PC<sub>igicuc</sub> method.

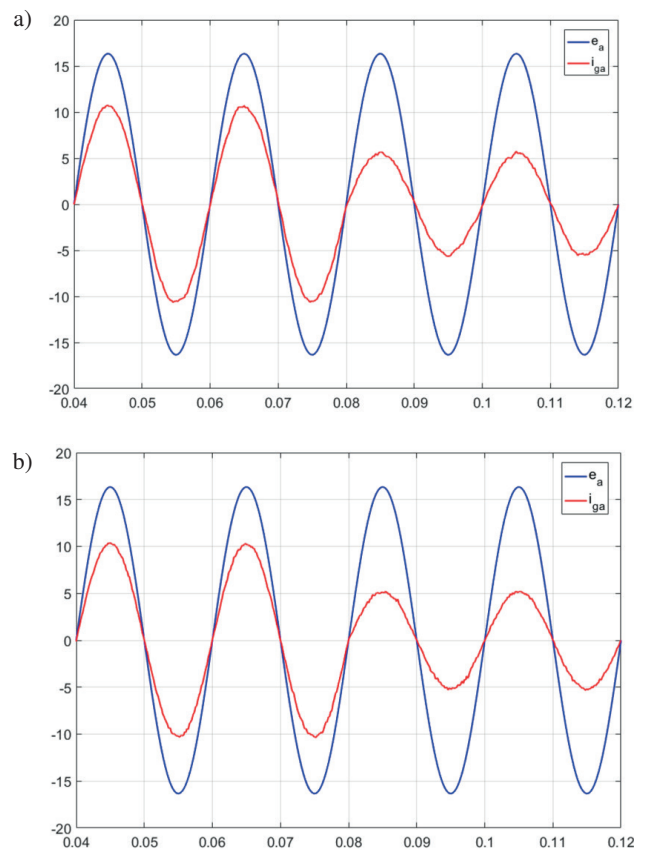


Fig. 14. Line phase voltage  $e_a$  (100 V/div) and current  $i_{ga}$  (5 A/div): a) PC<sub>icuc</sub>, b) PC<sub>igicuc</sub> for active power  $P = 5.0$  kW and 2.5 kW

The proposed manner of determining factors allows to estimate nominal values  $w_{ucN}$  and  $w_{igN}$ . The determined factors do not ensure the lowest THD<sub>i</sub> of the line current (the highest quality of current  $i_g$ ). The nominal values still be corrected in simulation tests. However, they allow to significantly reduce the time of implementation of the two methods (PC<sub>icuc</sub> and PC<sub>igicuc</sub>)

because they narrow down the search area for the best values. This method (i.e. relating the largest changes of the controlled values to each other) has also been used for the predictive torque control method (PTC).

## 5. Laboratory investigations

Practical implementation was performed on a 2-level active rectifier. The parameters of the experimental setup were the same as those presented for the simulation in Table 1. The values of weighting factors were  $w_{uc} = 1.0$  ( $PC_{i_{cu_c}}$ ) as well as  $w_{uc} = 1.0$  and  $w_{ig} = 24.3$  ( $PC_{i_{gic_{u_c}}}$ ). Characteristics of the laboratory setup are presented in Table 3. In practical implementation, the dead time was  $t_d = 3 \mu s$ , real power  $P = 5$  kW, and reactive power  $Q = 0$  Var. Experimental implementation included compensation of the calculation delay.

Table 3  
Main devices of the laboratory setup

Device	Model
Power analyzer	Yokogawa WT 1800
AC power supply	California MX30-3PI
Digital control	ADSP-21369 + XC3S400 FPGA

**5.1. Steady state waveforms.**  $THD_i$  and average switching frequency  $f_{sw(av)}$  are shown in Table 4. The waveforms of line voltage  $e_a$  and current  $i_{ga}$  in a steady state are shown in Fig. 15. Weight factor  $w_{ig}$  influences the quality of line current  $i_g$ , and the value of  $w_{uc}$  determines the damping level of resonance har-

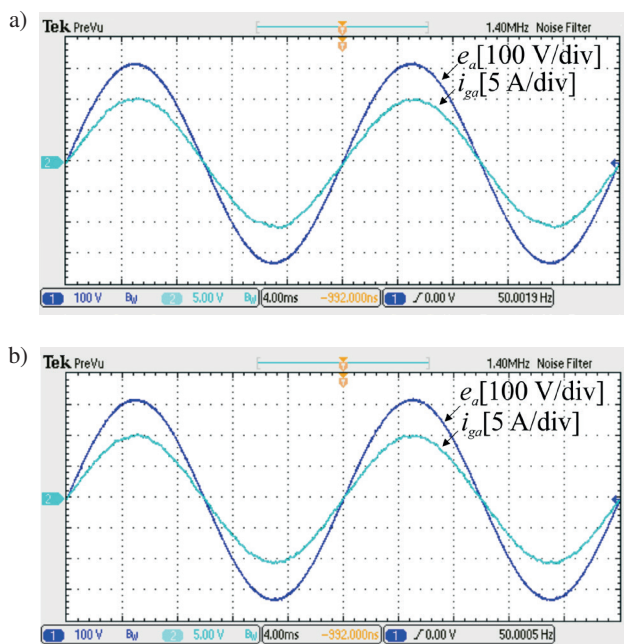


Fig. 15. Grid line voltage  $e_a$  (100 V/div) and current  $i_{ga}$  (5 A/div) for an algorithms: a)  $PC_{i_{cu_c}}$ ; b)  $PC_{i_{gic_{u_c}}}$  (test results)

monics. For the  $PC_{i_{gic_{u_c}}}$  control method with extended cost function (23) the value of  $THD_i$  was smaller than for  $PC_{i_{cu_c}}$ .

Table 4  
 $THD_i$  in steady state

Algorithm	$THD_i$ [%]	$f_{sw(av)}$ [kHz]
$PC_{i_{cu_c}}$	2.1	5.6
$PC_{i_{gic_{u_c}}}$	1.45	5.5

**5.2. Operation during transients.** To verify the effectiveness of control schemes and the calculation of weighting factors, tests were performed during transients. Oscilloscope measurements (Fig. 16) show grid voltage  $e_a$  and current  $i_{ga}$ , grid cur-

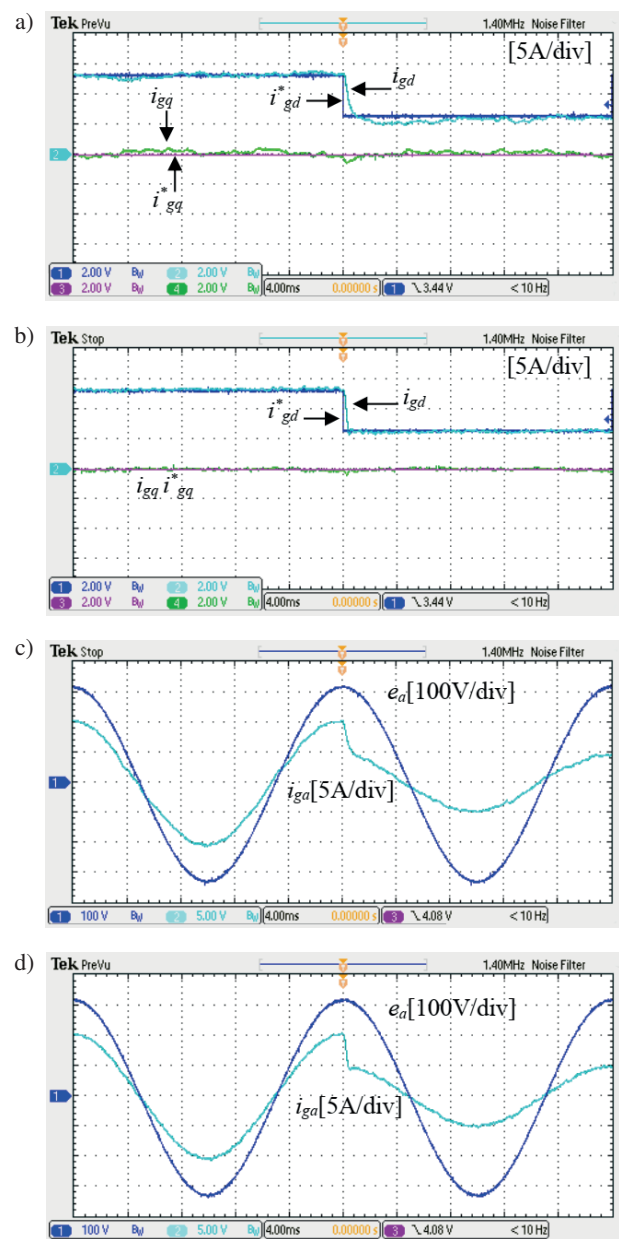


Fig. 16. Laboratory test results for variation of reference grid current vector components  $i_{gd}^*$  from 10 A to 5 A: a), c)  $PC_{i_{cu_c}}$ ; b), d)  $PC_{i_{gic_{u_c}}}$

rent vector components  $i_{gd}$ ,  $i_{gq}$  and their references  $i_{gd}^*$ ,  $i_{gq}^*$  during a step change of  $i_{gd}^*$  (proportional to active power) from 10 A to 5 A. It can be seen that the chosen values of weighting factors ensure not only effective performance during steady states but also in the case of dynamic changes of reference values.

**5.3. Operation under unbalanced network.** One of the most common power supply disruptions is voltage asymmetry. Most commonly the line voltage becomes unbalanced as a result of single-phase load, voltage dip, line impedance asymmetry, etc. The case in which a-phase voltage is decreased to 75% of the nominal value (Table 1) was examined to confirm robustness of the algorithms being investigated.

The waveforms of line current  $i_g$  and voltage  $e$  under unbalanced power supply are shown in Fig. 17. The THD<sub>i</sub> values of the line current and average switching frequency  $f_{sw(av)}$  are listed in Table 5. In both methods, the line current is balanced.

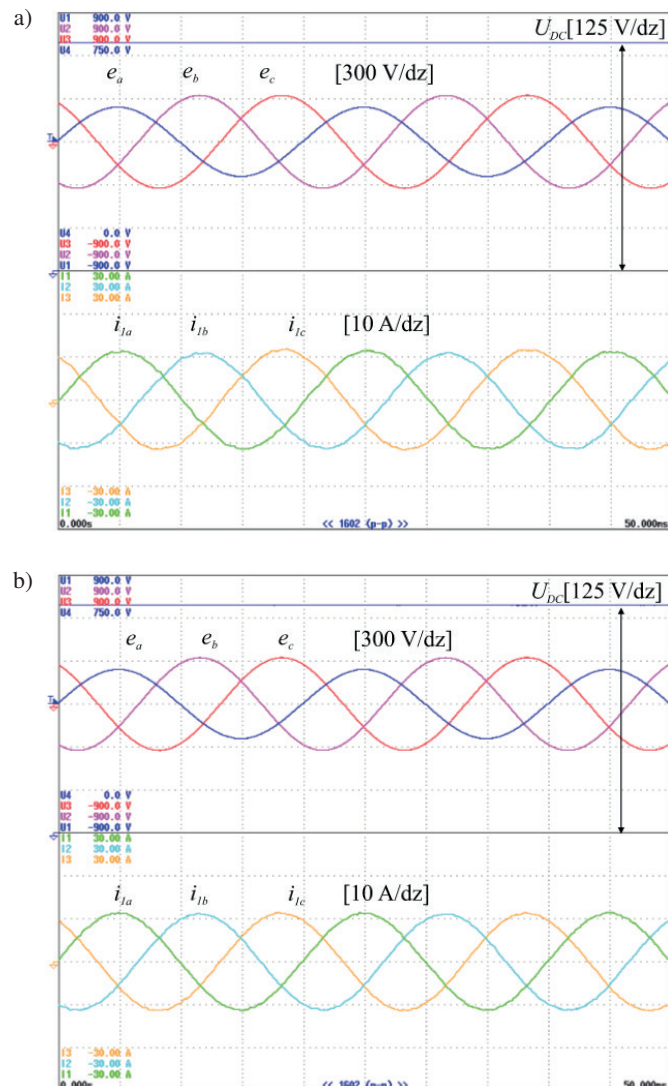


Fig. 17. Laboratory test results of converter operating with line voltage asymmetry. DC voltage, line voltages and currents for the algorithms: a) PCi<sub>c</sub>u<sub>c</sub>; b) PCi<sub>g</sub>i<sub>c</sub>u<sub>c</sub>

A lower THD<sub>i</sub> = 1.2% of the line current was obtained for the PCi<sub>g</sub>i<sub>c</sub>u<sub>c</sub> method. Experimental studies confirm that the values of coefficients  $w_{uc}$  and  $w_{ig}$ , determined in the manner described above, guarantee the operation of algorithms both in the case of balanced and unbalanced line voltage. It should be noted that THD<sub>i</sub> values are lower than for a steady state (Table 4). This is due to the fact that lower voltage in phase  $a$  causes the increase of the reference line current to supply the DC circuit with the same power  $P$ . At higher current values, a natural decrease in the value of THD<sub>i</sub> is observed.

Table 5  
THD<sub>i</sub> in steady state

Algorithm	THD <sub>i</sub> [%]	$f_{sw(av)}$ [kHz]
PCi <sub>c</sub> u <sub>c</sub>	1.8	5.5
PCi <sub>g</sub> i <sub>c</sub> u <sub>c</sub>	1.2	5.4

## 6. Conclusions

The paper compares two control methods (PCi<sub>c</sub>u<sub>c</sub> and PCi<sub>g</sub>i<sub>c</sub>u<sub>c</sub>) proposed to control the three-phase active rectifier with LCL filters. Both methods use one of the advantages of FCS-MPC method, i.e. simultaneous regulation of different parameters in a single cost function, which allows to essentially suppress the harmonics around LCL resonance in the line current. This paper presents simulations which were performed to verify the equations developed to predict the controlled quantities  $i_g$ ,  $i_c$  and  $u_c$ . This step is often overlooked by the authors of predictive methods. The results obtained confirm high accuracy of this manner of determining predicted values which, after the prediction time, coincide with the measured values. Another element presented in the publication is the description of how to select the optimum values of weighting factors  $w_{uc}$  and  $w_{ig}$ . There are basically no universal analytical methods for determining the values of weighting factors in the cost function in literature. The weighting factors calculated as presented in the paper are very close to the values giving the lowest THD<sub>i</sub> of the line current. The algorithm introduced allows us to significantly speed up the process of implementation of the presented methods. Experimental tests proved that the presented control algorithms with the weighting factors  $w_{uc}$  and  $w_{ig}$  calculated in the manner described above ensure excellent performance under both balanced and unbalanced line voltage conditions.

**Acknowledgements.** The work was supported by research project S/WE/1/2018 funded by the Polish Ministry of Science and Higher Education.

## REFERENCES

- [1] S. Vazquez, J. Rodriguez, M. Rivera, L.G. Franquelo and M. Norambuena, "Model Predictive Control for Power Converters and Drives: Advances and Trends", *IEEE Transactions on Industrial Electronics* 64 (2), 935–947 (2017).
- [2] J. Rodriguez et al., "State of the Art of Finite Control Set Model Predictive Control in Power Electronics", *IEEE Transactions on Industrial Informatics* 9 (2), 1003–1016 (2013).

- [3] D. du Toit, H. d. T. Mouton, R. Kennel and P. Stolze, “Predictive Control of Series Stacked Flying-Capacitor Active Rectifiers”, *IEEE Transactions on Industrial Informatics* 9 (2), 697–707 (2013).
- [4] K. Antoniewicz and K. Rafal, “Model predictive current control method for four-leg three-level converter operating as shunt active power filter and grid connected inverter”, *Bull. Pol. Ac.: Tech.* 65 (5), 601–607 (2017).
- [5] O. Sandre-Hernandez, J. d. J. Rangel-Magdaleno and R. Morales-Caporal, “Modified model predictive torque control for a PMSM-drive with torque ripple minimisation”, *IET Power Electronics* 12 (5), 1033–1042 (2019).
- [6] A. Dekka, B. Wu, V. Yaramasu, and N.R. Zargari, “Integrated model predictive control with reduced switching frequency for modular multilevel converters”, *IET Electr. Power Appl.* 11 (5), 857–863 (2017).
- [7] C. A. Rojas, M. Aguirre, S. Kouro, T. Geyer and E. Gutierrez, “Leakage Current Mitigation in Photovoltaic String Inverter Using Predictive Control With Fixed Average Switching Frequency”, *IEEE Transactions on Industrial Electronics* 64 (2), 9344–9354 (2017).
- [8] V. Yaramasu, B. Wu, M. Rivera, M. Narimani, S. Kouro and J. Rodriguez, “Generalised approach for predictive control with common-mode voltage mitigation in multilevel diode-clamped converters”, *IET Power Electronics* 8 (8), 1440–1450 (2015).
- [9] A.A. Ahmed, B.K. Koh and Y.I. Lee, “A Comparison of Finite Control Set and Continuous Control Set Model Predictive Control Schemes for Speed Control of Induction Motors”, *IEEE Transactions on Industrial Informatics* 14 (4), 1334–1346 (2018).
- [10] P. Wiatr and A. Kryński, “Model predictive control of multilevel cascaded converter with boosting capability – experimental results”, *Bull. Pol. Ac.: Tech.* 65 (5), 589–599 (2017).
- [11] A. Godlewska, “Control of the Current Source Rectifier using Finite Control Set Model Predictive Control”, *2017 19th Eur. Conf. Power Electron. Appl.*, 2017, 1–10.
- [12] K. Antoniewicz, M. Jasinski, M.P. Kazmierkowski and M. Malinowski, “Model Predictive Control for Three-Level Four-Leg Flying Capacitor Converter Operating as Shunt Active Power Filter”, *IEEE Transactions on Industrial Electronics* 63 (8), 5255–5262 (2016).
- [13] J. Scoltock, T. Geyer and U. Madawala, “Model Predictive Direct Current Control for a grid-connected converter: LCL-filter versus L-filter”, *2013 IEEE International Conference on Industrial Technology (ICIT)*, Cape Town, 2013, 576–581.
- [14] W. Wu, Y. Liu, Y. He, H.S. Chung, M. Liserre and F. Blaabjerg, “Damping Methods for Resonances Caused by LCL-Filter-Based Current-Controlled Grid-Tied Power Inverters: An Overview”, *IEEE Transactions on Industrial Electronics* 64 (9), 7402–7413 (2017).
- [15] N. Panten, N. Hoffmann and F.W. Fuchs, “Finite Control Set Model Predictive Current Control for Grid-Connected Voltage-Source Converters With LCL Filters: A Study Based on Different State Feedbacks”, *IEEE Transactions on Power Electronics* 31 (7), 5189–5200 (2016).
- [16] P. Falkowski and A. Sikorski, “Finite Control Set Model Predictive Control for Grid-Connected AC–DC Converters With LCL Filter”, *IEEE Transactions on Industrial Electronics* 65 (4), 2844–2852 (2018).
- [17] P. Cortes et al., “Guidelines for weighting factors design in Model Predictive Control of power converters and driven”, *2009 IEEE International Conference on Industrial Technology*, Gippsland, VIC, 2009, 1-7.
- [18] N. Hoffmann, F. W. Fuchs, M.P. Kazmierkowski and D. Schröder, “Digital current control in a rotating reference frame – Part I: System modeling and the discrete time-domain current controller with improved decoupling capabilities”, *IEEE Transactions on Power Electronics* 31 (7), 5290–5305 (2016).
- [19] F. Wang, S. Li, X. Mei, W. Xie, J. Rodríguez and R.M. Kennel, “Model-Based Predictive Direct Control Strategies for Electrical Drives: An Experimental Evaluation of PTC and PCC Methods”, *IEEE Transactions on Industrial Informatics* 11 (3), 671–681 (2015).
- [20] P. Zanchetta, “Heuristic multi-objective optimization for cost function weights selection in finite states model predictive control”, *2011 Workshop on Predictive Control of Electrical Drives and Power Electronics*, Munich, 2011, 70–75.
- [21] F. Villarroel, J.R. Espinoza, C.A. Rojas, J. Rodriguez, M. Rivera, and D. Sbarbaro, “Multiobjective switching state selector for finite-states model predictive control based on fuzzy decision making in a matrix converter”, *IEEE Transactions on Industrial Electronics* 60 (2), 589–599, (2013).
- [22] T.J. Vyncke, S. Thielemans and J.A. Melkebeek, “Finite-Set Model-Based Predictive Control for Flying-Capacitor Converters: Cost Function Design and Efficient FPGA Implementation”, *IEEE Transactions on Industrial Informatics* 9 (2), 1113–1121 (2013).
- [23] Y. Zhang and H. Yang, “Two-Vector-Based Model Predictive Torque Control Without Weighting Factors for Induction Motor Drives”, *IEEE Transactions on Power Electronics* 31 (2), 1381–1390 (2016).
- [24] C.A. Rojas, J. Rodriguez, F. Villarroel, J.R. Espinoza, C.A. Silva and M. Trincado, “Predictive Torque and Flux Control Without Weighting Factors”, *IEEE Transactions on Industrial Electronics* 60 (2), 681–690 (2013).
- [25] T. Dragičević and M. Novak, “Weighting Factor Design in Model Predictive Control of Power Electronic Converters: An Artificial Neural Network Approach”, *IEEE Transactions on Industrial Electronics* 66 (11), 8870–8880 (2019).
- [26] T. Geyer, “Algebraic Tuning Guidelines for Model Predictive Torque and Flux Control”, *IEEE Transactions on Industry Applications* 54 (5), 4464–4475 (2018).
- [27] L. A. Serpa, S. Ponnaluri, P.M. Barbosa and J.W. Kolar, “A Modified Direct Power Control Strategy Allowing the Connection of Three-Phase Inverters to the Grid Through LCL Filters”, *IEEE Transactions on Industry Applications* 43 (5), 1388–1400 (2007).
- [28] X. Zhang, Y. Wang, C. Yu, L. Guo and R. Cao, “Hysteresis Model Predictive Control for High-Power Grid-Connected Inverters With Output LCL Filter”, *IEEE Transactions on Industrial Electronics* 63 (1), 246–256 (2016).
- [29] A. Godlewska, R. Grodzki, P. Falkowski, M. Korzeniewski, K. Kulikowski, and A. Sikorski, “Advanced Control Methods of DC/AC and AC/DC Power Converters – Look-Up Table and Predictive Algorithms”, in *Advanced Control of Electrical Drives and Power Electronic Converters*, J. Kabzinski, Ed. Cham: Springer International Publishing, 221–302, 2017.